LETTER

doi:10.1038/nature10942

Resonant quantum transitions in trapped antihydrogen atoms

C. Amole[1], M. D. Ashkezari[2], M. Baquero-Ruiz[3], W. Bertsche[4,5,6], P. D. Bowe[7], E. Butler[8], A. Capra[1], C. L. Cesar[9], M. Charlton[4], A. Deller[4], P. H. Donnan[10], S. Eriksson[4], J. Fajans[3,11], T. Friesen[12], M. C. Fujiwara[12,13], D. R. Gill[13], A. Gutierrez[14], J. S. Hangst[7], W. N. Hardy[14,15], M. E. Hayden[2], A. J. Humphries[4], C. A. Isaac[4], S. Jonsell[16], L. Kurchaninov[13], A. Little[3], N. Madsen[4], J. T. K. McKenna[17], S. Menary[1], S. C. Napoli[4], P. Nolan[17], K. Olchanski[13], A. Olin[13,18], P. Pusa[17], C. Ø. Rasmussen[7], F. Robicheaux[10], E. Sarid[19], C. R. Shields[4], D. M. Silveira[20]†, S. Stracka[13], C. So[3], R. I. Thompson[12], D. P. van der Werf[4] & J. S. Wurtele[3,11]

The hydrogen atom is one of the most important and influential model systems in modern physics. Attempts to understand its spectrum are inextricably linked to the early history and development of quantum mechanics. The hydrogen atom's stature lies in its simplicity and in the accuracy with which its spectrum can be measured[1] and compared to theory. Today its spectrum remains a valuable tool for determining the values of fundamental constants and for challenging the limits of modern physics, including the validity of quantum electrodynamics and—by comparison with measurements on its antimatter counterpart, antihydrogen—the validity of CPT (charge conjugation, parity and time reversal) symmetry. Here we report spectroscopy of a pure antimatter atom, demonstrating resonant quantum transitions in antihydrogen. We have manipulated the internal spin state[2,3] of antihydrogen atoms so as to induce magnetic resonance transitions between hyperfine levels of the positronic ground state. We used resonant microwave radiation to flip the spin of the positron in antihydrogen atoms that were magnetically trapped[4–6] in the ALPHA apparatus. The spin flip causes trapped anti-atoms to be ejected from the trap. We look for evidence of resonant interaction by comparing the survival rate of trapped atoms irradiated with microwaves on-resonance to that of atoms subjected to microwaves that are off-resonance. In one variant of the experiment, we detect 23 atoms that survive in 110 trapping attempts with microwaves off-resonance (0.21 per attempt), and only two atoms that survive in 103 attempts with microwaves on-resonance (0.02 per attempt). We also describe the direct detection of the annihilation of antihydrogen atoms ejected by the microwaves.

Magnetostatic trapping of neutral atoms[7] or anti-atoms is accomplished by creating a local minimum of the magnetic field magnitude in free space. The confining force results from interaction of the atomic magnetic moment $\boldsymbol{\mu}$ with the non-uniform magnetic field. Figure 1 shows the expected Breit–Rabi hyperfine level diagram for the ground state of the antihydrogen atom in a magnetic field. We label the four eigenstates $|a\rangle$, $|b\rangle$, $|c\rangle$ and $|d\rangle$ in order of increasing energy. Trapping is possible when the atom is in a 'low-field seeking' quantum state ($|c\rangle$ or $|d\rangle$ in Fig. 1). We employ the Ioffe–Pritchard[7] configuration: the superposition of a magnetic multipole (an octupole) field that confines atoms in the transverse directions and two 'mirror coil' fields for axial confinement[8].

Working at the Antiproton Decelerator[9] facility at CERN, we recently demonstrated magnetic confinement of cold antihydrogen atoms[4] and showed that—once trapped—these atoms end up in their ground state, where they can be held[5] for up to 1,000 s. Here we use the same apparatus, modified to enable injection of microwaves into the trapping volume (Fig. 2a). Antihydrogen atoms are produced near the field minimum (about 1 T, Fig. 2b) by mixing cold plasmas of antiprotons and positrons for about 1 s (Methods). Atoms having kinetic energies corresponding to less than 0.5 K can be trapped. Mixing about two million positrons and 20,000 antiprotons yields approximately 6,000 anti-atoms; on average, approximately one anti-atom is trapped. The trapping field currents can be ramped down with a time constant of 9 ms, releasing trapped atoms in a well-defined time window[4]. The trapping volume is surrounded by a three-layer, 30,720-channel imaging silicon detector[10], which can locate the spatial positions—vertices—of antiproton annihilations.

Our approach was to subject trapped antihydrogen atoms to resonant microwaves to eject them from the trap. A tuned, oscillating magnetic field $\mathbf{B}_1$ applied perpendicularly to the trapping field can drive positron spin-flip transitions between the trappable and the untrappable states, that is, $|c\rangle \rightarrow |b\rangle$ and $|d\rangle \rightarrow |a\rangle$. Untrapped atoms escape and annihilate on the surrounding apparatus. A single experimental cycle or 'trapping attempt' involves producing anti-atoms in

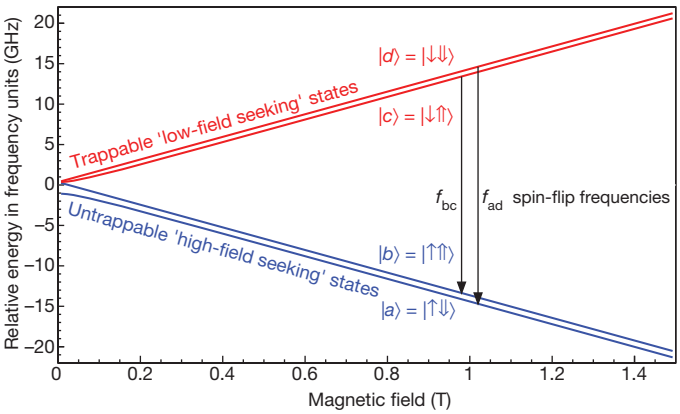

Figure 1 | Hyperfine energy levels. The Breit–Rabi diagram, showing the relative hyperfine energy levels of the ground state of the hydrogen (and antihydrogen, assuming CPT invariance) atom in a magnetic field. In the state vectors shown (for the high-field limit), the single arrow refers to the positron spin and the double arrow refers to the antiproton spin.

[1]Department of Physics and Astronomy, York University, Toronto, Ontario, M3J 1P3, Canada. [2]Department of Physics, Simon Fraser University, Burnaby, British Columbia, V5A 1S6, Canada. [3]Department of Physics, University of California, Berkeley, California 94720-7300, USA. [4]Department of Physics, Swansea University, Swansea SA2 8PP, UK. [5]School of Physics and Astronomy, University of Manchester, M13 9PL Manchester, UK. [6]The Cockcroft Institute, WA4 4AD Warrington, UK. [7]Department of Physics and Astronomy, Aarhus University, DK-8000 Aarhus C, Denmark. [8]CERN, Department PH, CH-1211 Geneva 23, Switzerland. [9]Instituto de Física, Universidade Federal do Rio de Janeiro, Rio de Janeiro 21941-972, Brazil. [10]Department of Physics, Auburn University, Auburn, Alabama 36849-5311, USA. [11]Lawrence Berkeley National Laboratory, Berkeley, California 94720, USA. [12]Department of Physics and Astronomy, University of Calgary, Calgary, Alberta T2N 1N4, Canada. [13]TRIUMF, 4004 Wesbrook Mall, Vancouver, British Columbia V6T 2A3, Canada. [14]Department of Physics and Astronomy, University of British Columbia, Vancouver, British Columbia V6T 1Z1, Canada. [15]The Canadian Institute of Advanced Research, Toronto M5G-1Z8, Canada. [16]Department of Physics, Stockholm University, SE-10691, Stockholm, Sweden. [17]Department of Physics, University of Liverpool, Liverpool L69 7ZE, UK. [18]Department of Physics and Astronomy, University of Victoria, Victoria, British Columbia V8W 3P6, Canada. [19]Department of Physics, NRCN-Nuclear Research Center Negev, Beer Sheva, IL-84190, Israel. [20]Atomic Physics Laboratory, RIKEN, Saitama 351-0198, Japan. †Present address: Instituto de Física, Universidade Federal do Rio de Janeiro, Rio de Janeiro 21941-972, Brazil.

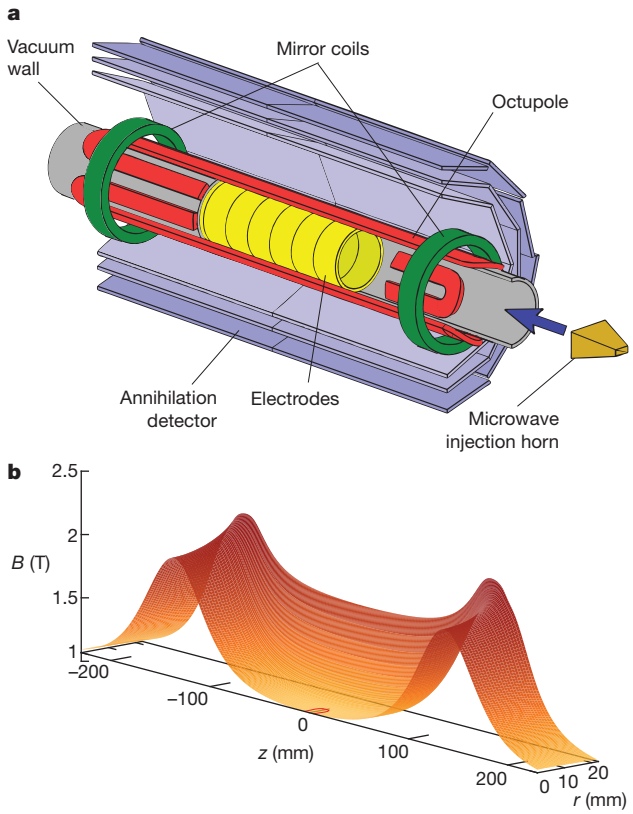

Figure 2 | The ALPHA device. **a**, Cut-away, schematic drawing of the antihydrogen synthesis and trapping region of the ALPHA apparatus. The superconducting atom-trap magnets, the annihilation detector, and some of the Penning trap electrodes are shown. An external solenoid (not shown) provides a 1-T magnetic field for the Penning trap. The drawing is not to scale. The inner diameter of the Penning trap electrodes is 44.5 mm and the minimum-B trap has an effective length of 274 mm. Microwaves are injected along the axis of the trapping volume using a horn antenna, which is located about 130 cm from the trap axial midpoint. **b**, Map of magnetic field strength in the ALPHA antihydrogen trap. The red contour bounds a region up to 0.35 mT (or 10 MHz in microwave frequency equivalent) above the minimum field, to roughly indicate the size of the resonant volume.

the magnetic trap, holding any trapped atoms first for 60 s (during which the magnetic field may be changed) and then for 180 s (during which microwaves may be introduced), and then intentionally releasing any remaining atoms to detect their annihilation.

To select the proper microwave frequencies and magnetic field configurations, we consider (Fig. 3a) the calculated positron spin resonance lineshapes for equal numbers of trapped $|c\rangle$ and $|d\rangle$ state atoms exposed to microwaves. The abrupt low-frequency onsets are associated with the minimum in the static magnetic field near the trap centre; the high-frequency tails reflect the highly inhomogeneous nature of the trapping fields elsewhere. We choose the resonance condition such that transitions are induced as atoms pass close to the magnetic minimum (Fig. 2b). This choice yields higher transition rates than elsewhere in the trap, and it localizes the position in space where transitions occur, and whence the resulting high-field seeking atoms are ejected. We do not know a priori the hyperfine level in which atoms are trapped; for a given magnetic field configuration we need to alternately irradiate the trap at two frequencies (details in Fig. 3 legend) separated by the zero-field hyperfine splitting of 1,420.4 MHz.

We collect two distinct, complementary types of annihilation data. First, at the end of every trapping attempt, we rapidly turn off the confining fields and watch for annihilation events in a 30-ms window from the start of the magnet shutdown. This allows us to determine an effective trapping rate. The ejection of trapped atoms by resonant microwaves will reduce this rate. Rates for application of resonant microwaves, off-resonant microwaves and no microwaves can be compared: these are 'disappearance mode' data. The second data set comes from monitoring annihilation events throughout the entire time that antihydrogen atoms are held in the trap. We look for events from ejected atoms during the time that resonant microwave fields are applied: these are 'appearance mode' data.

Because the duration of the observation window differs significantly between these two modes, we rely on two different cosmic background rejection algorithms (Methods). In the 30-ms 'disappearance window' we use the algorithm developed earlier[4] (the 'default criteria'). The rate at which cosmic ray events are interpreted as annihilations by this selection scheme is $(4.7 \pm 0.2) \times 10^{-2}\,\mathrm{s}^{-1}$. For the much longer 'appearance mode' observation (180 s), we rely on an alternative set of acceptance criteria that, compared to the default criteria, reduces annihilations by 25% but lowers the cosmic background by an order of magnitude. To avoid experimenter bias, the two sets of criteria are optimized and cross-checked using control samples[4,6]: cosmic ray events and annihilation events collected independently of the trapping experiments described here.

We conducted six series of measurements. For series 1, we set the minimum on-axis trapping field $B_{\mathrm{min}}^{\mathrm{axis}}$ to some value B^{A} (Methods), and then applied resonant microwave fields at frequencies $f_{\mathrm{bc}}^{\mathrm{A}}$ and $f_{\mathrm{ad}}^{\mathrm{A}}$ (Fig. 3b; see the legend for microwave frequency drive details) during the 180-s hold portion of the cycle. For series 2, we shifted $B_{\mathrm{min}}^{\mathrm{axis}}$ to $B^{\mathrm{B}} > B^{\mathrm{A}}$ by increasing the mirror coil currents such that microwave fields oscillating at $f_{\mathrm{bc}}^{\mathrm{A}}$ and $f_{\mathrm{ad}}^{\mathrm{A}}$ are detuned by 100 MHz and are no longer resonant with atoms at the centre of the trap (Fig. 3c). The field was shifted (in about 1 s) after the mixing and initial trapping phase of each trapping attempt, and a waiting period of 59 s was imposed to allow the field to stabilize before microwave introduction. This configuration should eliminate $|d\rangle \rightarrow |a\rangle$ transitions and reduce the rate of $|c\rangle \rightarrow |b\rangle$ transitions. The latter can still occur as atoms pass through regions of space in which the local magnetic field brings them into resonance with microwave fields applied at frequency $f_{\mathrm{ad}}^{\mathrm{A}}$. Series 3 involved operating at the higher field B^{B} and shifting the microwave frequencies so as to bring both transitions back into resonance (Fig. 3d). Series 4 field and frequency conditions were identical to those of series 2, but series 4 attempts were interleaved with those of series 3. This repetition attempts to minimize possible systematic effects due to time variations in the experimental conditions. Antiproton beam and plasma conditions—and thus the initial trapping rate—can vary from day to day, so on- and off-resonance experiments were interspersed. Thus, series 1 and 2 were taken under very similar conditions, and series 3 and 4 constitute a second, complementary set of measurements. In concert with series 1–4, we measured trapping and annihilation rates with $B_{\mathrm{min}}^{\mathrm{axis}}$ set to B^{A} or B^{B} when no microwaves are injected into the apparatus (series 5 and 6, respectively). Apart from changes in magnetic field or microwave conditions, the experimental procedure was identical for each of the six series.

A summary of 'disappearance mode' data appears in Tables 1 and 2. The errors quoted are based on counting statistics only. By comparing the Poisson rate of the process of interest with the rate of the control process, we evaluate the probability (P-value) that the observed number of outcomes, or a more extreme one, could have been produced by background fluctuations[11]. We observe a clear decrease in the survival rate for the cases in which microwaves are injected on-resonance, as compared to the equivalent off-resonance measurements, with a P-value of 1.0×10^{-5}.

The two measurement sets (series 1–2; series 3–4) could have different systematic uncertainties. For example, in the former, the mirror field shift might affect the orbit dynamics of the trapped antihydrogen (a hypothesis not supported by numerical simulations), while the latter could suffer from different microwave field characteristics between on- and off-resonance frequencies (again, this is not supported by our detailed off-line measurements with electron plasmas; see Methods). However, both data sets show decreases in the on-resonance rate

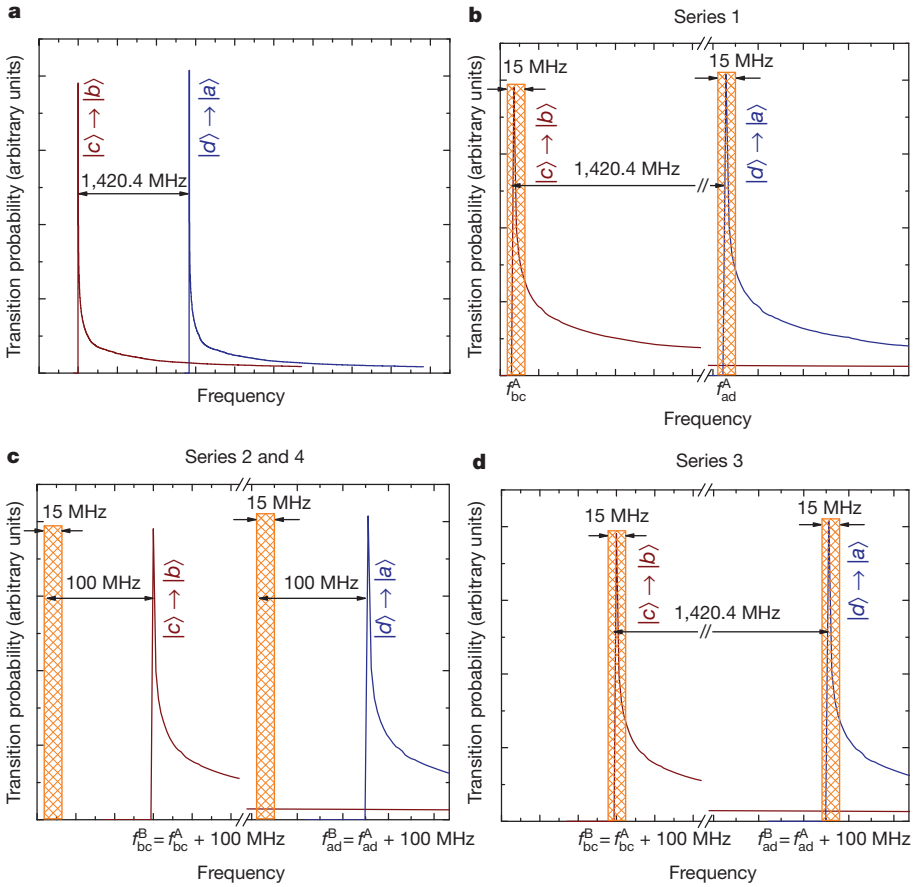

Figure 3 | Transition lineshapes and resonance conditions. **a**, Calculated spin-flip transition lineshapes in the ALPHA antihydrogen trap. Transition probability (arbitrary units) is plotted versus microwave frequency. Only the trapping field inhomogeneity is considered in calculating the lineshape. **b**, Schematic representation of the experimental situation for the on-resonance experiments at magnetic field B^A (series 1). The yellow bands represent the frequency ranges over which the microwaves are scanned. **c**, The situation for off-resonance experiments at magnetic field B^B (series 2 and 4). **d**, The situation for on-resonant experiments at magnetic field B^B (series 3). A two-segment frequency sweep lasting 30 s was used to apply microwave fields. This sweep was repeated six times in each trapping attempt for a total microwave application time of 180 s, beginning 60 s after the end of antihydrogen formation. In each case, the first 15-s scan covers the lower yellow band and the second 15-s scan covers the upper yellow band. The bands span −5 MHz to +10 MHz about the target frequency.

measurements, compared to the associated off-resonance measurements, with P-values of 1.6×10^{-4} and 1.5×10^{-2}, respectively, supporting the hypothesis that the difference is due to spin flip.

We note that the survival rates for the no-microwave measurements are higher than for those in which microwaves are present but off-resonance (the P-value is 6×10^{-3}). This difference could be explained by far off-resonant interactions with the $|c\rangle$ state, assuming there is sufficient microwave power to induce spin flips in the long tails of the resonance lineshape (Fig. 3c). (See the discussion of the appearance mode data below.)

We also directly searched for annihilation signals of anti-atoms that are ejected from the trap after a spin-flip transition—the 'appearance mode' described above. Figure 4a shows the time history of events satisfying the alternative acceptance criteria and having $|z| < 6$ cm (Methods). In the first frequency sweep ($0 < t < 30$ s) we observe a significant excess of counts ($P = 2.8 \times 10^{-5}$) in on-resonance (series 1 plus series 3) compared to off-resonance attempts (series 2 plus series 4). Seven of the 19 events appearing in $0 < t < 15$ s (microwaves probing f_{bc}) occur in the first second; for $15 < t < 30$ s (probing f_{ad}) the first second has seven of 18 events. This suggests that the microwave power is sufficient to flip most of the spins during the first 30-s sweep, in agreement with numerical simulations of the transition rate (Methods). An investigation of power dependence indicated that a level as low as one-sixteenth of the nominal 700 mW injected (Methods) was still enough to eject the trapped atoms in the first 30-s sweep, again consistent with the simulations.

In the off-resonant experiments, we observe a mild excess of counts above the no-microwave case (series 5 plus series 6) with an associated $P = 5.6 \times 10^{-2}$. We interpret this excess to be due to the above-mentioned off-resonance interaction with the $|c\rangle$ state. This conclusion is supported by the fact that the events are in $15 < t < 30$ s (Fig. 4a), when the microwaves are probing the upper 15-MHz

Table 1 | Series summaries for the 'disappearance mode' analysis

Series	Relative microwave frequency	Relative magnetic field	Number of attempts	Antihydrogen detected at trap shutdown	Rate	Comment
1	0 MHz	0 mT ($B^{axis}_{min} = B^A$)	79	1	0.01 ± 0.01	On resonance (Fig. 3b)
2	0 MHz	+3.5 mT ($B^{axis}_{min} = B^B$)	88	16	0.18 ± 0.05	Off resonance (Fig. 3c)
3	+100 MHz	+3.5 mT ($B^{axis}_{min} = B^B$)	24	1	0.04 ± 0.04	On resonance (Fig. 3d)
4	0 MHz	+3.5 mT ($B^{axis}_{min} = B^B$)	22	7	0.32 ± 0.12	Off resonance (Fig. 3c)
5	Off	0 mT ($B^{axis}_{min} = B^A$)	52	17	0.33 ± 0.08	No microwaves
6	Off	+3.5 mT ($B^{axis}_{min} = B^B$)	48	23	0.48 ± 0.10	No microwaves

Table 2 | Totals for all 'disappearance mode' series

	Number of attempts	Detected antihydrogen	Rate
On resonance (1 + 3)	103	2	0.02 ± 0.01
Off resonance (2 + 4)	110	23	0.21 ± 0.04
No microwaves (5 + 6)	100	40	0.40 ± 0.06

frequency band (Fig. 3c), and by indications that the nominal power should be sufficient to drive off-resonant transitions. Taken together, the disappearance and appearance analyses constitute a consistent picture of the fate of the trapped antihydrogen atoms.

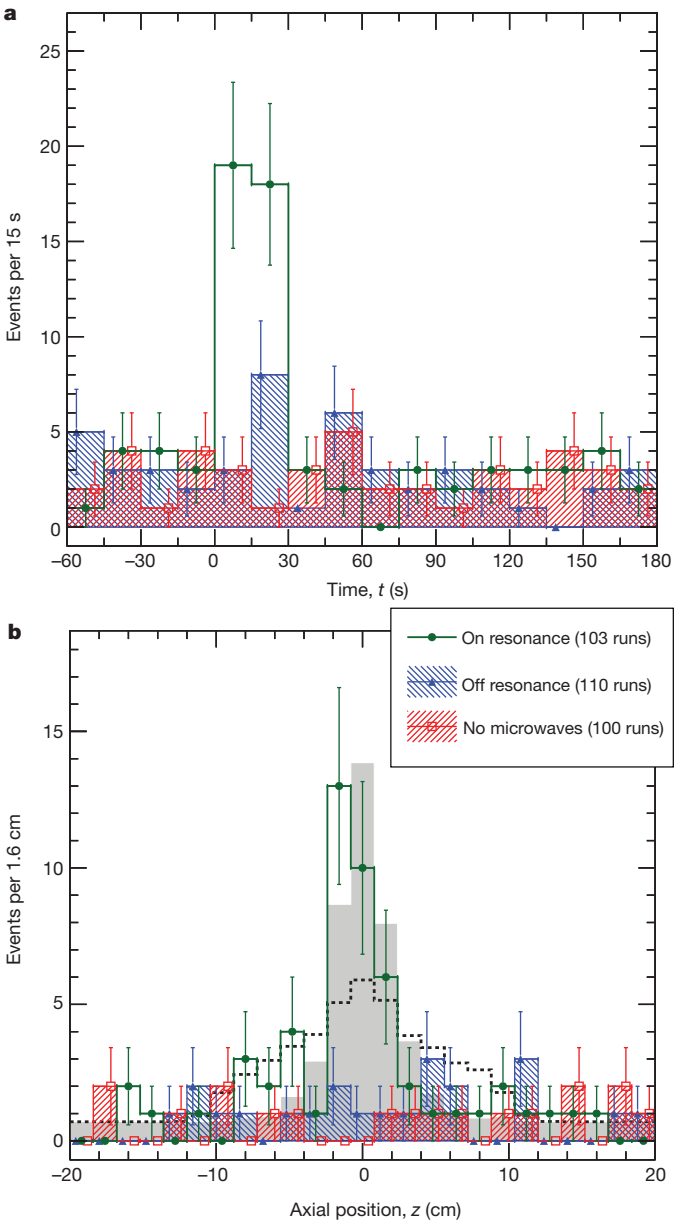

Figure 4 | Appearance mode data. a, The number of 'appearance mode' annihilation events satisfying the alternative selection criteria and $|z| < 6$ cm (Methods) as a function of time between the end of antihydrogen production and the trap shutdown. Microwave power is first applied at time $t = 0$. The expected cosmic background per bin per run is 0.026 ± 0.005 events. The error bars are due to counting statistics. **b**, The z-distribution of annihilation vertices in 'appearance mode' for $0 < t < 30$ s. The grey histogram is the result of a numerical simulation of the motion of spin-flipped atoms ejected from the trap. The dashed black curve is the result of a simulation of trapped antihydrogen annihilating on the residual gas (Methods). Both simulations are normalized to the on-resonant data.

We have considered other processes that could lead to antihydrogen loss in the presence of microwaves but that could not be due to a spin-flip. The only plausible candidate is heating of the trap electrodes by the microwaves, causing desorption from the surfaces of cryo-pumped material, which could then scatter or annihilate the trapped anti-atoms. Indeed, we observe a slight electrode temperature increase from about 8 K to at most 11 K during the 180-s microwave cycle. However, any such thermal effect on the vacuum should be the same for series 1 and 2, which differ only by a slight change in the trapping magnetic field. Further evidence against vacuum deterioration comes from Fig. 4b, which shows the z-distribution of appearance-type events (in $0 < t < 30$ s). The distribution is highly localized around the trap centre, as we expect from simulations of how spin-flipped atoms are lost from the trap (Methods). Annihilation or collisional loss of trapped anti-atoms in a compromised vacuum could occur anywhere in the 274-mm-long trapping volume.

We thus conclude that we have observed resonant interaction of microwave radiation with the internal quantum states of trapped antihydrogen atoms. This is a proof-of-principle experiment; we have not yet attempted to accurately localize a resonance or determine a spectroscopic lineshape. We have bounded the resonance between the off-resonance scan value and the maximum of the on-resonance sweep. Roughly speaking, the observed resonance is within 100 MHz of the resonance frequency expected for hydrogen, corresponding to a relative precision of about 4×10^{-3}. This experiment marks the advent of antimatter spectroscopy and takes a preliminary step towards precision comparison of the spectra of hydrogen and antihydrogen as a test of CPT symmetry. Importantly, it also demonstrates the viability of performing fundamental measurements on small numbers of trapped anti-atoms by combining resonant interaction with the long trapping times and sensitive annihilation detection in ALPHA. In future experiments, the transition $|c\rangle \leftrightarrow |d\rangle$ could be probed by double resonance; the frequency of this transition goes through a broad maximum[12] at a field of 0.65 T, allowing a precision measurement of hyperfine parameters without requiring precise knowledge of the absolute value of B (see Supplementary Information).

METHODS SUMMARY

The ALPHA apparatus traps antihydrogen atoms synthesized from cold plasmas of positrons and antiprotons. Microwaves from a frequency synthesizer were amplified and injected into the magnetic atom trap using a horn antenna. We use electron cyclotron frequency measurement techniques to set the magnetic field in the device, and to characterize microwave field patterns. We perform numerical simulations of trapped antihydrogen dynamics to model microwave resonant lineshapes and transition rates, atom ejection dynamics, and the spatial distribution of residual gas annihilation. Two distinct analysis methods are used to reduce cosmic ray background in the annihilation detector.

Full Methods and any associated references are available in the online version of the paper at www.nature.com/nature.

Received 9 January; accepted 7 February 2012.
Published online 7 March 2012.

1. Hänsch, T. W. Nobel lecture: Passion for precision. *Rev. Mod. Phys.* **78,** 1297–1309 (2006).
2. Martin, A. G., Helmerson, K., Bagnato, V. S., Lafyatis, G. P. & Pritchard, D. E. RF spectroscopy of trapped neutral atoms. *Phys. Rev. Lett.* **61,** 2431–2434 (1988).
3. Fujiwara, M. C. *et al.* Towards antihydrogen confinement with the ALPHA antihydrogen trap. *Hyperfine Interact.* **172,** 81–89 (2006).
4. Andresen, G. B. *et al.* Trapped antihydrogen. *Nature* **468,** 673–676 (2010).
5. Andresen, G. B. *et al.* Confinement of antihydrogen for 1,000 seconds. *Nature Phys.* **7,** 558–564 (2011).
6. Andresen, G. B. *et al.* Search for trapped antihydrogen. *Phys. Lett. B* **695,** 95–104 (2011).
7. Pritchard, D. E. Cooling neutral atoms in a magnetic trap for precision spectroscopy. *Phys. Rev. Lett.* **51,** 1336–1339 (1983).
8. Bertsche, W. *et al.* A magnetic trap for antihydrogen confinement. *Nucl. Instrum. Meth. A* **566,** 746–756 (2006).
9. Maury, S. The antiproton decelerator: AD. *Hyperfine Inter.* **109,** 43–52 (1997).
10. Andresen, G. B. *et al.* The ALPHA detector: module production and assembly. *J. Instrum.* **7,** C01051 (2012).

11. Przyborowski, J. & Wilenski, H. Homogeneity of results in testing samples from Poisson series. *Biometrika* **31,** 313–323 (1939).
12. Hardy, W. N. *et al.* Magnetic resonance studies of gaseous atomic hydrogen at low temperatures. *Phys. Rev. Lett.* **42,** 1042–1045 (1979).

Supplementary Information is linked to the online version of the paper at www.nature.com/nature.

Acknowledgements This work was supported by CNPq, FINEP/RENAFAE (Brazil), ISF (Israel), MEXT (Japan), FNU (Denmark), VR (Sweden), NSERC, NRC/TRIUMF, AITF, FQRNT (Canada), DOE, NSF (USA), EPSRC, the Royal Society and the Leverhulme Trust (UK). We thank them for their generous support. We are grateful to the AD team (T. Eriksson, P. Belochitskii, B. Dupuy, L. Bojtar, C. Oliveira, B. Lefort and G. Tranquille) for the delivery of a high-quality antiproton beam. We thank the following individuals for help: M. Harrison, J. Escallier, A. Marone, M. Anerella, A. Ghosh, B. Parker, G. Ganetis, J. Thornhill, D.Wells, D. Seddon, F. Butin, H. Brueker, K. Dahlerup-Pedersen, J. Mourao, T. Fowler, S. Russenschuck, R. De Oliveira, N. Wauquier, J. Hansen, M. Polini, J. M. Geisser, L. Deparis, P. Frichot, J. M. Malzacker, A. Briswalter, P. Moyret, S. Mathot, G. Favre, J. P. Brachet, P. Mésenge, S. Sgobba, A. Cherif, J. Bremer, J. Casas-Cubillos, N. Vauthier, G. Perinic, O. Pirotte, A. Perin, G. Perinic, B. Vullierme, D. Delkaris, N. Veillet, K. Barth, R. Consentino, S. Guido, L. Stewart, M. Malabaila, A. Mongelluzzo, P. Chiggiato, G. Willering, E. Mahner, A. Froton, C. Lasseur, F. Hahn, E. Søndergaard, F. Mikkelsen, W. Carlisle, A. Charman, J. Keller, P. Amaudruz, D. Bishop, R. Bula, K. Langton, P. Vincent, S. Chan, D. Rowbotham, P. Bennet, B. Evans, J.-P. Martin, P. Kowalski, A. Read, T. Willis, J. Kivell, H. Thomas, W. Lai, L. Wasilenko, C. Kolbeck, H. Malik, P. Genoa, L. Posada, R. Funakoshi, M. Okeane, S. Carey and N. Evetts. We thank former collaborators M. J. Jenkins, G. B. Andresen, R. Hydomako, S. Chapman, A. Povilus, R. Hayano, L. V. Jørgensen and Y. Yamazaki. We are grateful to the CERN Summer Student Program for funding the participation of undergraduate students (C.Ø.R. and S.C.N.) in our experiment.

Author Contributions W.B., P.D.B., J.F., M.C.F., J.S.H., N.M. and D.M.S. conceived, designed and constructed the central ALPHA apparatus and participated in all aspects of the experimental and physics programme. The microwave hardware was designed and fabricated by M.D.A., E.B., W.N.H. and M.E.H., who also participated in all aspects of the experimental programme. T.F. developed the electron cyclotron resonance diagnostic and participated actively in all aspects of the experimental programme. S.S. developed the alternative event analysis and participated actively in the experimental and analysis efforts. C.A., M.B.-R., A.C., A.G., A.J.H., J.T.K.M., E.S. and C.S. participated actively in the experimental runs, data taking, on- and offline analysis, and maintenance and modification of the apparatus. D.R.G. and A.O. contributed to all aspects of the detector systems and participated actively in the experimental shift work and analysis efforts. M.C. designed and built the positron accumulator and participated in the experimental shift work, the physics planning effort, and the strategic direction of the experiment. D.P.v.d.W. designed and built the positron accumulator, contributed to the magnetic design of the atom trap, and participated in the experimental programme. F.R., with help from P.H.D., performed the spin-flip simulations reported in this paper and supported the design and experimental programme with simulations and calculations. P.N. led the design of the ALPHA silicon detector. P.P. was responsible for implementing the silicon detector at CERN and participated in the experimental and analysis programme. A.D., C.A.I., C.Ø.R., S.C.N., A.L. and C.R.S. contributed to the experimental shift work. S.J. and J.S.W. contributed theoretical support in the form of atomic or plasma physics calculations and simulations and contributed to the experimental shift work. C.L.C., S.E., S.M. and R.I.T. participated in the experimental programme and the physics planning effort. L.K. and K.O. provided offsite support for detector electronics and database management systems, respectively, and contributed to the experimental shift work. E.B., J.S.H. and M.E.H. wrote the initial manuscript, which was edited, improved and approved by the entire collaboration.

Author Information Reprints and permissions information is available at www.nature.com/reprints. The authors declare no competing financial interests. Readers are welcome to comment on the online version of this article at www.nature.com/nature. Correspondence and requests for materials should be addressed to J.S.H. (hangst@phys.au.dk) or M.E.H. (mhayden@sfu.ca).

METHODS

Antihydrogen synthesis and trapping. The ALPHA techniques for synthesizing trappable anti-atoms are described extensively elsewhere[4–6]. Antihydrogen atoms are produced near the trap minimum by mixing cold plasmas of antiprotons and positrons for about 1 s in a Penning–Malmberg[13] trap. The mixing makes use of the evaporative cooling[14] (for both positrons and antiprotons) and autoresonant injection[15] techniques developed for our initial demonstration of trapping. At the end of the 1-s synthesis stage the magnetic trap fields are on and the trapping region has been cleared of any remaining charged particles. The anti-atoms are then held in the trap for 240 s before being released. During the first 1 s of this time period we either ramp the mirror coil currents from 650 A to 692 A (adding 3.5 mT to $B_{\mathrm{min}}^{\mathrm{axis}}$ to attain B^{B}), or do nothing (to remain at B^{A}). During the next 59 s we wait to ensure that the currents in the mirror coils have stabilized. Finally, during the last 180 s we either inject microwaves or not, depending on the measurement type.

Microwave injection. Ka-band microwaves from an Agilent 8257D PSG Signal Generator are amplified and injected down the axis of the apparatus via a waveguide-fed horn antenna. The maximum power used was about 700 mW, measured at the vacuum transition.

Electron cyclotron resonance diagnostics. We measure the electron cyclotron resonance frequency by loading an electron plasma in the centre of the trap. A series of 4-μs microwave pulses is injected, at frequencies scanned across the cyclotron resonance; these pulses heat the plasma. Between each pulse we allow the plasma to return to its equilibrium temperature. Simultaneously, we monitor the quadrupole vibrational mode of the plasma by applying an oscillating potential at 26.5 MHz to an electrode adjacent to the plasma and measuring the plasma response on another. The frequency of this mode shifts approximately linearly with changes in temperature[16]. When the microwave frequency matches the cyclotron frequency, the heating of the plasma and the quadrupole frequency shift will be maximized. This method allows us to determine and to set the trapping magnetic field and to ensure field stability between trapping attempts.

Using the quadrupole frequency shift diagnostic, we can also infer the *in situ* amplitude of the microwave electric fields near the trap centre. We adjust the solenoid field so that the electron cyclotron resonance frequency is equal to one of the spin-flip transition frequencies and inject resonant microwave pulses to heat the plasma. From the temperature increase we can infer that the peak electric field amplitudes for 700 mW injected power are about $E(f_{\mathrm{bc}}^{\mathrm{A}}) = 110\ \mathrm{V\,m^{-1}}$, $E(f_{\mathrm{ad}}^{\mathrm{A}}) = 150\ \mathrm{V\,m^{-1}}$, $E(f_{\mathrm{bc}}^{\mathrm{B}}) = 130\ \mathrm{V\,m^{-1}}$, $E(f_{\mathrm{ad}}^{\mathrm{B}}) = 100\ \mathrm{V\,m^{-1}}$.

In yet another mode of operation, we fix the microwave frequency and apply an axial magnetic field gradient across a long (about 4 cm) electron plasma so that only a narrow slice of the plasma is in resonance. The external solenoid field is then swept through resonance to generate a map of electric field strength along the length of the plasma, reflecting the underlying standing-wave pattern. This provides another check of the similarity of microwave field distributions at the four frequencies, as well as of variations over the 15-MHz frequency sweeps. We see no evidence for significant differences in the microwave environment at the two pairs of frequencies ($f_{\mathrm{bc}}^{\mathrm{A}}$, $f_{\mathrm{ad}}^{\mathrm{A}}$ and $f_{\mathrm{bc}}^{\mathrm{B}}$, $f_{\mathrm{ad}}^{\mathrm{B}}$) or within the sweeps.

Magnetic field settings. The background solenoid field of about 1 T is the same as that used previously[4]. We use the electron cyclotron resonance technique to quantify the contributions of the solenoid and trap magnets to $B_{\mathrm{min}}^{\mathrm{axis}}$ and to determine the field change necessary to achieve the 100 MHz offset for off-resonant operation. The microwave frequencies used for driving ($f_{\mathrm{bc}}^{\mathrm{A}}$, $f_{\mathrm{ad}}^{\mathrm{A}}$) were (28.276, 29.696) GHz and for ($f_{\mathrm{bc}}^{\mathrm{B}}$, $f_{\mathrm{ad}}^{\mathrm{B}}$) were (28.376, 29.796) GHz. The electron cyclotron resonance measurements were used to monitor field stability from attempt to attempt; any necessary corrections were done by adjusting the background solenoid field. The reproducibility of the field-setting procedure translates to ±2 MHz in microwave frequency.

Numerical simulations of antihydrogen dynamics. We use a mixture of quantum and classical mechanics to simulate the effect of the microwaves on the trapped antihydrogen, and to calculate spatial distributions, both for ejected atoms, and for atoms lost by annihilation on the residual gas. The simulated anti-atoms[4] are in a low-field seeking state and are launched from the region of the positron plasma with a 50 K thermal distribution; only those with kinetic energy less than about 0.5 K are trapped. The atomic motion is calculated classically using a smooth fit to the magnetic field to obtain the centre-of-mass force.

The spatial structure of the microwave field in the electrode stack is complex, but an order-of-magnitude estimate of spin-flip transition rates can be obtained by assuming that the microwave magnetic fields $\mathbf{B_1}$ are those of a plane wave propagating in free space. During each simulation time step, we check whether the spin-flip resonance condition was met. If it was, we compute the transition probability from the standard Landau–Zener approximation for a two state system using a three-point time fit to the energy and coupling parameters. In the strong trapping field, the coupling matrix element between the states is approximately $B_1\mu/4$. The resonance condition is met twice each time the atom passes through the centre of the trap, and we allow for the unlikely possibility of the spin flipping twice. The coupling matrix element V can be related to the Rabi frequency, $\Omega = V/\hbar$. For a microwave electric field of $100\ \mathrm{V\,m^{-1}}$ (giving a vacuum intensity of $1.3\ \mathrm{mW\,cm^{-2}}$), B_1 is about 0.33 μT and the Rabi frequency is approximately $1.5 \times 10^4\ \mathrm{rad\,s^{-1}}$. Simulations do not lead to a simple exponential decay of trapped population when the microwaves are present, because antihydrogen trajectories differ in how they pass through the resonance volume. As a rough estimate, a microwave intensity of $2\ \mathrm{mW\,cm^{-2}}$ gives a flip rate of the order of $1\ \mathrm{s^{-1}}$.

Default criteria for annihilation event identification. The detector tracks the trajectories of charged pions that are produced when released antihydrogen atoms encounter matter in the Penning trap electrodes and annihilate. A reconstruction algorithm that considers track topology is then used to discriminate between pion tracks and cosmic ray events, and ultimately to locate the spatial position ('vertex') of each annihilation event[17]. The detector and the 'default criteria' for the event discrimination procedure have been extensively described previously[6,17].

Alternative criteria for annihilation event identification. We use a bagged decision tree classifier, in the random forest approach[18–20], to separate antiproton annihilations on the trap walls from cosmic ray events. Nine variables are used for classification: (1) the radial and (2) the azimuthal coordinates of the reconstructed annihilation vertex, if present, (3) the total number of channels registering 'hits' by charged particles, (4) the number of three-hit combinations used as track candidates, (5) the number of reconstructed tracks, (6) the sum of the squared residual distances of hits from a fitted straight line, and three topological variables. The topological variables comprise (7) a sphericity variable, (8) the cosine of the angle between the event axis and the detector axis, and (9) the angle between the vertical and the projection of the event axis onto the transverse $(x-y)$ plane. The sphericity variable is defined as the quantity $\frac{3}{2}(\lambda_2 + \lambda_3)$. Here $\lambda_1 \geq \lambda_2 \geq \lambda_3$ are the eigenvalues of the tensor $S^{\alpha\beta} = \left(\sum_i^N p_i^\alpha p_i^\beta |\mathbf{p}_i|^{-2}\right) \Big/ N$, where p_i^α is the component α (where $\alpha = x,y,z$) of the momentum associated with the ith track. The event axis is defined as the line passing through the centre of the detector and oriented along the eigenvector associated with λ_1.

The random forest event-selection criteria have been determined by maximizing a sensitivity figure of merit[21]. Compared to the 'default' selection, this method is about ten times more effective in rejecting cosmic background, while retaining 75% of the signal. For Fig. 4a, based on dynamical simulations, we require the event's axial position z to be less than 6 cm away from the trap centre. This requirement affects the signal only marginally and further suppresses the background by a factor of three, resulting in a cosmic rate of $(1.7 \pm 0.3) \times 10^{-3}\ \mathrm{s^{-1}}$. For Fig. 4b we select an annihilation candidate if it falls within $0 < t < 30$ s (the first microwave sweep).

13. Dehmelt, H. Nobel lecture: experiments with an isolated subatomic particle at rest. *Rev. Mod. Phys.* **62,** 525–530 (1990).
14. Andresen, G. B. *et al.* Evaporative cooling of antiprotons to cryogenic temperatures. *Phys. Rev. Lett.* **105,** 013003 (2010).
15. Andresen, G. B. *et al.* Autoresonant excitation of antiproton plasmas. *Phys. Rev. Lett.* **106,** 025002 (2011).
16. Tinkle, M. D., Greaves, R. G., Surko, C. M., Spencer, R. L. & Mason, G. W. Low-order modes as diagnostics of spheroidal non-neutral plasmas. *Phys. Rev. Lett.* **72,** 352–355 (1994).
17. Andresen, G. B. *et al.* Antihydrogen annihilation reconstruction with the ALPHA silicon detector. *Nucl. Instrum. Meth. A* (submitted).
18. Breiman, L. Random forests. *Mach. Learn.* **45,** 5–32 (2001).
19. Narsky, I. StatPatternRecognition: a C++ package for statistical analysis of high energy physics data. Preprint at http://arxiv.org/abs/physics/0507143 (2005).
20. Narsky, I. Optimization of signal significance by bagging decision trees. Preprint at http://arxiv.org/abs/physics/0507157 (2005).
21. Punzi, G. Sensitivity of searches for new signals and its optimization. In *Proc. PHYSTAT2003: Statistical Problems in Particle Physics, Astrophysics, and Cosmology* 79–83 Preprint at http://arxiv.org/abs/physics/0308063 (2003).